Applied Physics Express **5** (2012) 014101
DOI: 10.1143/APEX.5.014101

Single-Wire Light-Emitting Diodes Based on GaN Wires Containing Both Polar and Nonpolar InGaN/GaN Quantum Wells

Gwénolé Jacopin, Andrés De Luna Bugallo, Pierre Lavenus, Lorenzo Rigutti*, François H. Julien, Luiz F. Zagonel[1,2], Mathieu Kociak[1], Christophe Durand[3], Damien Salomon[3,4], Xiao Jun Chen[3], Joël Eymery[3], and Maria Tchernycheva

Institut d'Electronique Fondamentale UMR CNRS 8622, University Paris Sud 11, 91405 Orsay Cedex, France
[1]*Laboratoire de Physique des Solides, UMR CNRS 8502, University Paris Sud 11, 91405 Orsay Cedex, France*
[2]*Laboratório Nacional de Nanotecnologia—Centro Nacional de Pesquisa em Energia e Materiais, 13083-970, Campinas, Brazil*
[3]*Equipe mixte "Nanophysique et semiconducteurs", CEA/CNRS/Université Joseph Fourier, SP2M, UMR-E CEA/UJF-Grenoble 1, INAC, 17 rue des Martyrs, 38054 Grenoble Cedex 9, France*
[4]*CEA-Leti, MINATEC Campus, 38054 Grenoble, France*

Received November 15, 2011; accepted November 22, 2011; published online December 16, 2011

Single-wire light-emitting diodes based on radial p–i–n multi quantum well (QW) junctions have been realized from GaN wires grown by catalyst-free metal organic vapor phase epitaxy. The $In_xGa_{1-x}N$/GaN undoped QW system is coated over both the nonpolar lateral sidewalls and on the polar upper surface. Cathodo- and electroluminescence (EL) experiments provide evidence that the polar QWs emit in the visible spectral range at systematically lower energy than the nonpolar QWs. The EL of the polar or nonpolar QWs can be selectively activated by varying the sample temperature and current injection level. © 2012 The Japan Society of Applied Physics

Visible-to-UV light-emitting diodes (LEDs) based on nitride nanowires (NWs) have attracted much attention in the last few years due to their potential as highly efficient and cost-effective light sources.[1–3] First, axial InGaN/GaN quantum disc NW-based LEDs have been demonstrated.[1,2] Then, in order to benefit from the large surface area of the NWs, LEDs using radial InGaN/GaN quantum wells (QWs) coated on both polar and semi-polar lateral facets were fabricated.[3] A recent study demonstrated LEDs based on NW ensembles containing nonpolar, semipolar and polar QWs.[4] Our groups have recently demonstrated ensemble-based[5] and single-wire[6] LEDs based on radial and axial p–i–n multi QW(MQW) junctions containing nonpolar radial and polar axial QWs. In this work, we investigate the interplay between the contributions of both junctions. The devices are realized from n-type GaN wires grown by catalyst-free metal organic vapor phase epitaxy (MOVPE) coated at their top by five $In_xGa_{1-x}N$/GaN undoped QWs and by a p-doped GaN shell. The QW system is formed over both the nonpolar lateral sidewalls and on the polar upper surface. Cathodo- (CL) and electroluminescence (EL) experiments reveal that the polar QWs emit in the visible spectral range at systematically lower energy ($E = 2.25$–2.75 eV, depending on the In content) than the nonpolar QWs ($E = 2.6$–3.1 eV). The EL of the polar QWs is observed at room temperature and at a low current level, while the nonpolar QWs become dominant at low temperature and at higher injection current. We explain these observations by considering the system as consisting of two different LEDs contacted in parallel, corresponding to the polar and nonpolar p–i–n junctions.

Self-assembled *c*-oriented GaN wires having lateral $\{1\bar{1}00\}$ *m*-plane facets have been grown by MOVPE on *c*-sapphire substrates as described in detail in refs. 6–9. The base of the wires is grown at 1000 °C using trimethylgallium (TMG) and ammonia precursors as well as silane addition to obtain n^{++}-doping and to promote the wire geometry. The silane addition is switched off after about 15 μm length to grow an unintentionally doped GaN part (about 10 μm long) at the top of the wires. The GaN wires are coated at their top with five unintentionally doped radial InGaN/GaN QWs. Two samples (samples 1 and 2) have been grown at different InGaN growth temperatures ($T_1 = 710$ °C, $T_2 = 750$ °C, respectively) in order to obtain QWs with various In composition. The resulting composition in the radial QWs are of 24% in sample 1 and 16% in sample 2, according to the calibration based on spatially resolved seondary ion mass spectrometry (SIMS) measurements.[6] The scanning electron microscopy (SEM) image in Fig. 1(a) shows a typical as-grown wire from the sample 2. The heterojunction scheme is illustrated in Fig. 1(b). The transmission electron microscopy (TEM) investigation of a longitudinal slice from the top of the wire [Fig. 1(b)] reveals that InGaN is deposited on both the upper wire surface and on the lateral sidewalls. This yields both axial (polar) and radial (nonpolar) MQW systems. The growth times have been set in order to obtain well and barrier thicknesses equal to 1 nm (±0.2 nm) and 8 nm (±1 nm), respectively, for the radial MQW system, as confirmed by TEM measurements.[6] Finally, a p-doped GaN

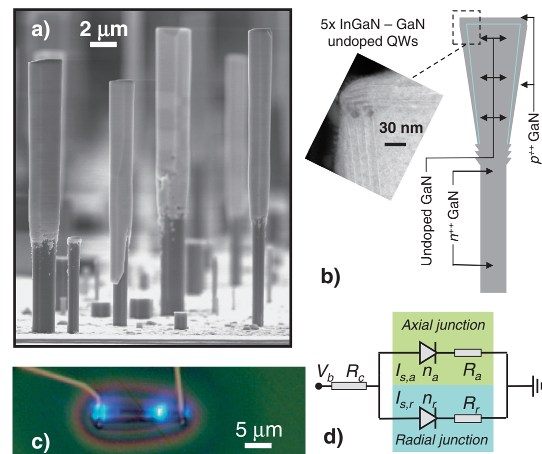

Fig. 1. (a) SEM image of as-grown wires from sample 2; (b) scheme of the wire heterostructure and TEM image of the top region of the wires, showing the presence of radial and axial quantum wells; (c) optical microscopy image of a processed nanowire emitting blue light under forward bias; (d) scheme illustrating the two-junction model used to interpret the EL properties.

*E-mail address: lorenzo.rigutti@ief.u-psud.fr

 © 2012 The Japan Society of Applied Physics

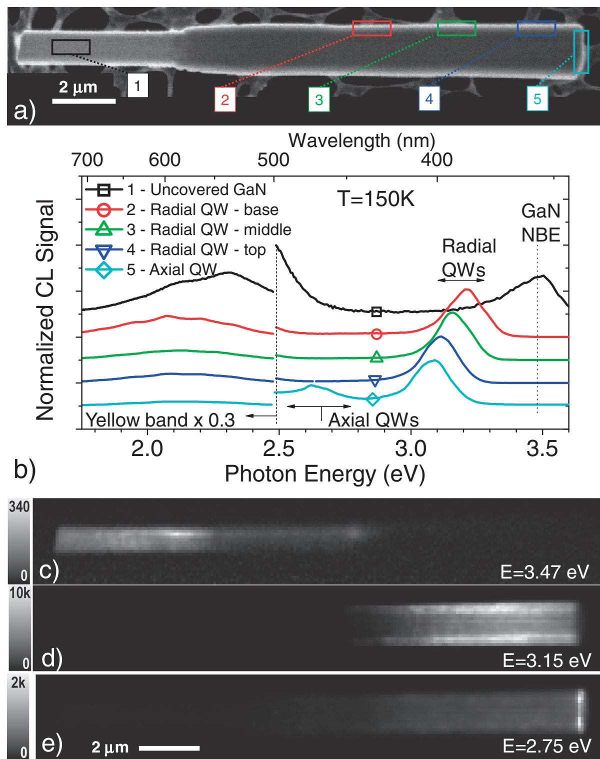

Fig. 2. (a) Dark-field image of a wire from sample 2 analyzed by CL-STEM; (b) CL spectra collected from the regions marked in (a); spectra are normalized and vertically shifted for clarity. (c) CL map at $E = 3.47$ eV; (d) at $E = 3.15$ eV; (e) at $E = 2.75$ eV.

shell grown at 920 °C in N_2 is added on the MQWs using biscyclopentadienylmagnesium as a precursor source with an annealing step performed under N_2 at 750 °C for 20 min to activate Mg dopants.

The optical properties of the wires have been investigated using a CL system with maximized collection angle and high spectral resolution.[10] The system uses a 300 mm optical spectrometer and a charge-coupled-device (CCD) camera for parallel spectra acquisition (spectral resolution of 1 nm), installed in a VG HB 501 scanning transmission electron microscope (STEM). The STEM is operated at 60 kV with a probe current of about 300 pA. The sample stage temperature is maintained at 150 K by liquid nitrogen cooling. For each pixel of the image, a full CL spectrum is recorded, with typical dwell times per pixel equal to 150 ms.

The dark-field STEM image of a wire from sample 2 oriented with the *m*-plane facets $\{1\bar{1}00\}$ parallel to the impinging beam is shown in Fig. 2(a). The GaN base part can be recognized on the left-hand side. The spectra of the different wire regions are displayed in Fig. 2(b). The spectrum of the uncovered base [labelled region 1 in Fig. 2(a)] shows the emission of the GaN near-band edge (NBE) at an energy of 3.47 eV and a broad yellow/green defect band peaked at around 2.35 eV. The spectra of the radial MQW system show an intense emission in the UV, gradually shifting from 3.10 eV close to the wire base (region 2) to 3.21 eV close to the wire top (region 4). Finally, the spectrum extracted by exciting the very top of the wire (region 5) is quite similar to that of region 4, except for the peak at 2.65 eV. In all the spectra an intense broad yellow band is present, peaked at around 2.3 eV in the heavily n-doped wire base and at 2.15 eV in the unintentionally doped regions.[11] The spatial distribution of the different spectral components is reported in the CL monochromatic images in Figs. 2(c)–2(e), obtained by putting in each pixel of the image the intensity of the corresponding spectrum at the corresponding energy. The GaN NBE emission at 3.47 eV [Fig. 2(c)] is clearly distinguishable only in the uncovered n-type base. The UV emission around 3.15 eV [Fig. 2(d)] becomes more intense when the beam approaches the lateral facets and can thus be attributed to the radial nonpolar QWs.[6,9] The spectral shift observed from region 2 to 4 can be ascribed to a QW thickness gradient, as confirmed by separate spatially resolved SIMS in samples grown by the present technique.[6] Figure 2(e) reports the spatial distribution of the signal at 2.65 eV. This spectral component is strongly concentrated on the very top of the wire, which justifies its attribution to the emission of the axial polar QWs. The lower transition energy with respect to the radial nonpolar QWs can be partly explained with the quantum-confined Stark effect related to the presence of an internal electric field in the axial QWs. Furthermore, the In content and well thickness in the axial QWs may be significantly larger than those in the lateral QWs.[6]

Single-wire LEDs were fabricated using wire dispersion on a Si/SiO_2 template, planarization in spin-on glass (H-silsequioxane), and electron-beam lithography, as described in ref. 9. The contacts to the single-wire devices have been fabricated by a double run of e-beam lithography, using a Ti/Al/Ti/Au (Ni/Au) metallization for the n-type (p-type) extremity of the wire. As the MQW system is coated only on the upper wire part leaving the n-type stem uncovered at the base, no intermediate etching of the core is necessary.[12] The optical microscopy image of a single-wire LED from sample 2 emitting blue light at RT under a forward current $I = 3$ µA is shown in Fig. 1(c). An average of 10 wires per sample have been processed and subsequently studied. In the following, we will refer to single-wire devices whose features are representative of the corresponding sample.

The EL of single-wire LEDs has been measured at room temperature (RT) and at different current levels by analyzing the light in a 460-mm-focal-length grating spectrometer with a CCD array, with a spectral resolution of 1 nm. Two series of EL spectra recorded at RT and for increasing injection levels are reported in Figs. 3(a)–3(b), corresponding to a single wire LED from samples 1 and 2, respectively. In both cases, there is a visible EL peak appearing at a low injection current ($I \leq 1$ µA). As the current is increased, the visible peak saturates and is progressively masked by a second peak growing at higher energy. The lower-energy peaks are on the average at 2.25 ± 0.10 eV in sample 1 and at 2.70 ± 0.15 eV in sample 2. The higher-energy contributions are peaked at 2.61 ± 0.13 eV in sample 1 and at 3.12 ± 0.15 eV in sample 2. The blue shift of the EL emission peaks in sample 2 with respect to sample 1 is attributed to the smaller In content. Comparison between the CL and EL data for sample 2 shows that the EL peak at 2.60 eV (resp., 3.1–3.2 eV) well correlates to the axial (resp., radial) MQW CL emission. As the temperature is decreased, the low-energy emission from the axial MQWs becomes weaker, while the

© 2012 The Japan Society of Applied Physics

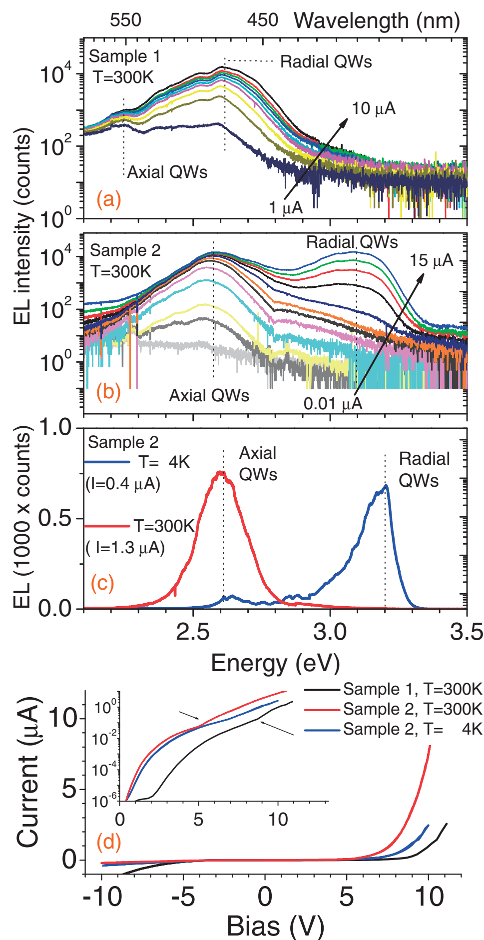

Fig. 3. (a, b) RT injection-dependent electroluminescence spectra collected from single-wire LEDs from samples 1 and 2. (c) EL spectra from a single-wire LED from sample 2 at different temperatures. (d) I–V curves of a wire from sample 1 at RT, from sample 3 at $T = 4$ K and RT; the inset shows the same characteristics in semilogarithmic scale.

emission of the radial MQWs increases even at low injection current, as shown in the case of the wire from sample 2 in Fig. 3(c). At large injection current (15 µA), the emission of the radial MQWs dominates at RT.

These optoelectronic properties can be interpreted by approximating the single-wire device as consisting of a radial and an axial p–i–n junction contacted in parallel, as illustrated by the equivalent scheme in Fig. 1(d). The spectral properties of the EL depend on which MQW system is preferentially injected with carriers, as pointed out for the NW ensemble LEDs of ref. 4. Current–voltage (I–V) curves of the devices analyzed by EL are shown in Fig. 3(d). The RT I–V curves show that the devices are rectifying. Some parts of the curves can be fitted by an exponential with high ideality factors ($n_{id} > 10$).[13] The nonexponential parts of the curves indicate that high series resistance values (tens of MΩ) determine the diode characteristics. It must be noticed that for current levels in the range of 0.1–1 µA, the slope of the RT I–V curve rapidly increases with increasing forward bias, as pointed out by the arrows in the inset to Fig. 3(d). We attribute this behaviour to the onset of current injection into the radial junction. This indicates either a higher series resistance or a lower ideality factor for the axial junction with respect to the radial junction. In any case, the low-T I–V curves [as shown in Fig. 3(d)] for sample 2 do not exhibit such slope discontinuity as those at RT, which indicates an overall increase of the series resistance, most likely in the p-type layer. These effects may be related to the resistance of the p-type GaN layer separating the metal contact from the axial junction. As the latter is more distant from the metal p-type contact, we suggest that the increase of the series resistance with decreasing temperature due to acceptor de-activation is larger for the axial junction than for the radial junction. Therefore, only the EL from the radial MQWs is observed at low T.

In summary, we have studied core-shell single wire p–i–n junction LEDs containing both an axial polar and a radial nonpolar InGaN/GaN MQW system. Spatially resolved CL indicates that the axial MQWs emit visible light at lower energy than the radial MQW system. Only the axial polar MQWs are activated at RT with current $I \leq 1$ µA. When the current level is increased, carriers are more efficiently injected into the radial nonpolar MQWs, whose EL peak becomes progressively dominant. Finally, the energy of the peak related to both MQW systems can be tuned by varying the In content in the QWs during growth.

Acknowledgments This work was supported by the French ANR Agency under Programs Nos. ANR-08-NANO-031 BoNaFO and ANR-08-BLAN-0179 NanoPhotoNit. The authors thank M. Terrier for FIB preparation, C. Bougerol for TEM observations, and A. L. Bavencove for preliminary CL results and fruitful discussion. X.J.C. thanks the foundation "Nanosciences aux limites de la nanoélectronique" for financial support.

1) A. Kikuchi, M. Kawai, M. Tada, and K. Kishino: Jpn. J. Appl. Phys. **43** (2004) L1524.
2) H. M. Kim, Y. H. Cho, H. Lee, S. I. Kim, S. R. Ryu, D. Y. Kim, T. W. Kang, and K. S. Chung: Nano Lett. **4** (2004) 1059.
3) F. Qian, S. Gradecak, Y. Li, C. Y. Wen, and C. M. Lieber: Nano Lett. **5** (2005) 2287.
4) Y. J. Hong, C. H. Lee, A. Yoon, M. Kim, H. K. Seong, H. J. Chung, C. Sone, Y. J. Park, and G. C. Yi: Adv. Mater. **23** (2011) 3284.
5) A.-L. Bavencove, D. Salomon, M. Lafossas, B. Martin, A. Dussaigne, F. Levy, B. André, P. Ferret, C. Durand, J. Eymery, Le Si Dang, and P. Gilet: Electron. Lett. **47** (2011) 765.
6) R. Koester, J. Hwang, D. Salomon, X. J. Chen, C. Bougerol, J.-P. Barnes, D. Le Si Dang, G. Jacopin, A. De Luna Bugallo, L. Rigutti, M. Tchernycheva, C. Durand, and J. Eymery: Nano Lett. **11** (2011) 4839.
7) R. Koester, J. S. Hwang, C. Durand, D. Le Si Dang, and J. Eymery: Nanotechnology **21** (2010) 015602.
8) X. J. Chen, G. Perillat-Merceroz, D. Sam-Giao, C. Durand, and J. Eymery: Appl. Phys. Lett. **97** (2010) 151909.
9) A. De Luna Bugallo, L. Rigutti, G. Jacopin, F. H. Julien, C. Durand, X. J. Chen, D. Salomon, J. Eymery, and M. Tchernycheva: Appl. Phys. Lett. **98** (2011) 233107.
10) L. F. Zagonel, S. Mazzucco, M. Tencé, K. March, R. Bernard, B. Laslier, G. Jacopin, M. Tchernycheva, L. Rigutti, F. H. Julien, R. Songmuang, and M. Kociak: Nano Lett. **11** (2011) 568.
11) M. A. Reshchikov and H. Morkoç: J. Appl. Phys. **97** (2005) 061301.
12) F. Qian, Y. Li, S. Gradecak, H. G. Park, Y. J. Dong, Y. Ding, Z. L. Wang, and C. M. Lieber: Nat. Mater. **7** (2008) 701.
13) D. Zhu, J. Xu, A. N. Noemaun, J. K. Kim, E. F. Schubert, M. H. Crawford, and D. D. Koleske: Appl. Phys. Lett. **94** (2009) 081113.

© 2012 The Japan Society of Applied Physics